AGU PUBLICATIONS

JGR

Journal of Geophysical Research: Space Physics

RESEARCH ARTICLE
10.1002/2016JA022854

Key Points:
- EMEC instability is studied with quasi-linear theory for the first time
- Core and halo electrons mutually interact during instability progression
- Macroscopic quasi-linear theory is a useful tool for studying solar wind electrons

Correspondence to:
P. H. Yoon,
yoonp@umd.edu

Citation:
Sarfraz, M., S. Saeed, P. H. Yoon, G. Abbas, and H. A. Shah (2016), Macroscopic quasi-linear theory of electromagnetic electron cyclotron instability associated with core and halo solar wind electrons, *J. Geophys. Res. Space Physics*, *121*, 9356–9368, doi:10.1002/2016JA022854.

Received 23 APR 2016
Accepted 4 OCT 2016
Accepted article online 7 OCT 2016
Published online 25 OCT 2016

Macroscopic quasi-linear theory of electromagnetic electron cyclotron instability associated with core and halo solar wind electrons

M. Sarfraz[1], Sundas Saeed[1], P. H. Yoon[2,3], G. Abbas[1], and H. A. Shah[4]

[1]Department of Physics, GC University Lahore, Lahore, Pakistan, [2]Institute for Physical Science and Technology, University of Maryland, College Park, Maryland, USA, [3]School of Space Research, Kyung Hee University, Yongin, South Korea, [4]GC University Lahore, Lahore, Pakistan

Abstract Spacecraft observations made near 1 AU show that both core and halo solar wind electrons exhibit temperature anisotropies that appear to be regulated by marginal electromagnetic electron cyclotron instability condition. In the literature, the threshold conditions of this instability, operative for $T_\perp > T_\parallel$, have been expressed as an inverse correlation between the temperature anisotropy, $T_\perp/T_\parallel$, and parallel beta, $\beta_\parallel$, but such a relation was deduced on the basis of linear stability analysis combined with empirical fitting. The present paper, on the other hand, employs macroscopic quasi-linear analysis for core-halo two-component model of the solar wind electrons, in order to follow the self-consistent time history of the core and halo temperature development as well as the dynamics of magnetic field perturbation wave energy. In the present analysis, the inverse correlation for core and halo temperature anisotropy and parallel beta naturally emerges from the solutions of self-consistent theory. The present findings indicate that the macroscopic quasi-linear method may be useful for modeling the dynamics of solar wind electrons.

1. Introduction

The solar wind plasmas are known to be weakly or almost collisionless and are pervaded by electromagnetic fields on a wide range of time and length scales [*Zimbardo et al.*, 2010; *Bruno*, 2013]. Previous theoretical and experimental investigations [*Feldman et al.*, 1975; *Gary et al.*, 1975; *Gary and Feldman* 1977; *Gary et al.*, 1994] suggest that temperature anisotropy instabilities may arise due to the outflow of thermal energy in the solar wind. In the radially expanding solar wind plasmas, density (n) and magnetic field intensity (B) decrease with radial distance r, following the scaling given by $n, B \propto r^{-2}$. Owing to thermal outflow of electrons, the classic CGL relations [*Chew et al.*, 1956] predict the spontaneous generation of an excessive parallel temperature anisotropy, $T_\parallel > T_\perp$, and increasing plasma beta as a function of r. However, measurements in the solar wind near 1 AU show that sometimes the opposite anisotropy, $T_\perp/T_\parallel > 1$, also characterizes the solar wind electrons. How such a perpendicular heating can occur is not clear, however.

If the plasma is stable to excitation of instabilities, then no enhanced fluctuations are expected, and no influence of collective processes on the macroscopic parameters is envisaged. In contrast, if the plasma evolution leads to an unstable state, the electromagnetic fields resulting from instabilities are then expected to play an important role in controlling the thermodynamics and transport of particles and energy [*Gary*, 1993].

The existence of temperature anisotropies (source of free energy) in the solar wind and in the magnetospheres are confirmed directly by in situ measurements for electrons, protons, and other ion species [*Marsch*, 2006; *Samsonov et al.*, 2007; *Štverák et al.*, 2008]. We are interested in the electron anisotropy-driven instabilities in the present paper. Observations show that the distribution of solar wind electrons can be modeled mainly by core, halo, and strahl (moving in antisunward direction) components [*Montgomery et al.*, 1968; *Feldman et al.*, 1975; *Gurgiolo et al.*, 2012; *Goldstein et al.*, 2015]. In general, for solar wind plasma at large heliospheric distances, the relative density of the strahl component is negligibly small $n_s \ll n_h \ll n_c$ (where n_c, n_h, and n_s are core, halo, and strahl number densities, respectively). It is also suggested that the strahl component gradually evolves into halo via pitch angle scattering, which seems to be supported by observations that show that the strahl and halo densities are inversely proportional to radial distance, while their sum remaining roughly

the same [*Maksimovic et al.*, 2005; *Štverák et al.*, 2009]. In the present study, we approximately treat the solar wind electrons as core-halo two-component model, since owing to their low density, the presence of strahl may not have much significant effect on our conclusion.

Of course, our assumption of ignoring the contribution of strahl implies that we do not consider possible effective parallel temperature owing to the strahl streaming velocity. Even though the strahl has low densities (1 to 2% of the total electron number density), its relatively high differential streaming velocity, which is much higher than the core thermal speed may be a major contributor to the heat flux and effective parallel temperature. Consequently, the present analysis is limited to only thermal anisotropies that are not driven by differential streaming effects.

The core electrons are highly dense and relatively cold, but the halo component is relatively less dense but with high thermal energy, with the condition typical of $n_c \gg n_h$. Both core and halo populations exhibit temperature anisotropies. In a recent investigation, *Lazar et al.* [2015] model the core population as an isotropic Maxwellian and halo with bi-Kappa distribution. In another paper, *Lazar et al.* [2014] assume core as anisotropic Maxwellian and halo as bi-Kappa distribution. They then carried out the linear stability analysis of the core-halo electron system subject to electromagnetic anisotropy-driven instabilities propagating in directions parallel to the ambient magnetic field. In a related work, *Eliasson and Lazar* [2015] carried out Vlasov simulation of electromagnetic electron-cyclotron instability for initial bi-Kappa electrons, but they adopted a single component electron model. The present paper is similar to the papers by *Lazar et al.* [2014, 2015] in that we adopt two-component electron model, except that we go beyond their linear analysis and include quasi-linear calculations. Our paper also complements the work by *Eliasson and Lazar* [2015] in that we discuss time evolution of two-component electrons in contrast to their single-component model.

From observed parameters from the solar wind, the core can be modeled rather well with the bi-Maxwellian model, but the halo component is better modeled by the Kappa distribution. However, the Kappa parameter based upon observations is in the range of 6 to 8. From the perspective of wave dispersion relation, such a range of Kappa parameters yields results that are practically similar to the bi-Maxwellian model calculation. We therefore assume that both the core and halo components are given by the bi-Maxwellian velocity distributions. Observations for such kind of two-component electron distribution comprising the anisotropic core and halo in the solar wind have been reported in the literature [see, e.g., *Feldman et al.*, 1975; *Pilipp et al.*, 1987; *Maksimovic et al.*, 2005; *Štverák et al.*, 2008, 2009].

Electromagnetic electron cyclotron (EMEC) instability exists in the high-frequency range, with the wave vector lying in parallel (and antiparallel) direction with respect to the ambient magnetic field. The instability is driven by perpendicular temperature anisotropy, $T_\perp > T_\parallel$ [*Hollweg and Völk*, 1970]. In the literature, the anisotropy-driven EMEC instability was studied by *Kennel and Petscheck* [1966], *Dum et al.* [1980], *Wu et al.* [1989], and *Schlickeiser et al.* [2011] for bi-Maxwellian electrons and by *Lazar et al.* [2011], *Lazar et al.* [2013], *Viñas et al.* [2014], and *Viñas et al.* [2015] for nonthermal electron population. For the opposite case of excessive parallel temperature, i.e., $T_\parallel > T_\perp$, the threshold conditions for electron firehose instability are discussed by *Hollweg and Völk* [1970], *Paesold and Benz* [1999], *Li and Habbal* [2000], and *Gary and Nishimura* [2003] for bi-Maxwellian species and *Lazar and Poedts* [2009], *Viñas et al.* [2015], and *Lazar et al.* [2016] investigated the same problem for non-Maxwellian electrons in both nonresonant and resonant cases. Also, *Gary and Wang* [1996] and *Xiao et al.* [2006] proposed inverse correlation between electron temperature anisotropy, $A = T_\perp / T_\parallel$, and electron beta, $\beta_\parallel$, as

$$A = 1 + \frac{a}{\beta_\parallel^b}, \tag{1}$$

where a and b are the fitting parameters that can be found in their papers. *Lazar et al.* [2015], however, suggested an improved relation,

$$A = 1 + \frac{a}{\beta_\parallel^b}\left(1 + \frac{c}{\beta_\parallel^d}\right), \tag{2}$$

where a, b, c, and d are the fitting parameters that can be found in Tables A1–A4 of the paper by *Lazar et al.* [2015]. *Gary and Wang* [1996] and *Xiao et al.* [2006] considered a single-component anisotropic electrons. In contrast, *Lazar et al.* [2014, 2015] extended the analysis to the core-halo two-component electron model.

These authors plotted the inverse correlation between anisotropy and plasma beta for both populations following methodology adapted by *Gary and Wang* [1996] and *Xiao et al.* [2006], except that they used improved empirical formula (2).

The aim of the paper is to go beyond linear theory and solve the self-consistent set of macroscopic quasi-linear kinetic equations for perpendicular and parallel temperatures and wave energy intensity for both core and halo populations of electrons. The basic methodology was already outlined by *Davidson and Ogden* [1975], who pioneered the method of macroscopic quasi-linear theory, but their work pertains to ion cyclotron instability. Nevertheless, the basic scheme can be trivially applied to the electron cyclotron instability. For instance, *Yoon et al.* [2012] employed such a method to investigate the quasi-linear evolution of electromagnetic electron cyclotron (or whistler) instability, but they considered a single anisotropic electron component. In the present paper, we consider two-component, core-halo electron populations, following *Lazar et al.* [2014, 2015], and it will be shown that the anisotropy of each population is mutually affected such that during the quasi-linear development of the instability, the anisotropies continually evolve. The present quasi-linear calculation is consistent with the empirical anisotropic-beta relation such as (1) or (2), since the saturation state of the quasi-linear evolution under the assumption of bi-Maxwellian electron distribution automatically corresponds to the marginal state of the system. Thus, the present macroscopic quasi-linear analysis confirms the empirical marginal stability threshold condition.

The present paper is organized as follows. In section 2, we briefly discuss the linear and quasi-linear theory of electromagnetic electron cyclotron instability. Numerical solutions are presented in section 3. In section 4, we summarizes the findings of the present paper.

2. Theoretical Formalism

In the present discussion, we assume bi-Maxwellian distribution for both core and halo electrons. We assume that the basic functional form remains unchanged for all times, except that perpendicular and parallel temperatures of electrons population (core and halo components) may vary in time,

$$f_a = \frac{1}{\pi^{3/2}\alpha_{\perp a}^2(t)\alpha_{\parallel a}(t)} \exp\left(-\frac{v_\perp^2}{\alpha_{\perp a}^2(t)} - \frac{v_\parallel^2}{\alpha_{\parallel a}^2(t)}\right), \tag{3}$$

where $a = c, h$ stands for core/halo. Of course, the above model for the electron distribution is an approximation, and for realistic situation, the velocity space distribution may be locally distorted and deviate from the bi-Maxwellian form. The readers should be aware of such a caveat.

Here we also ignore the net relative drift between the core and halo, which is sometimes observed, especially in the fast solar wind. The net relative drift between plasma components with magnitude higher than some threshold values plays a role of additional free energy source and thus can lead to instability growth [*Gary*, 1993]. Under the condition, $\mathbf{k} \times \mathbf{B_0} = 0$, for electromagnetic electron/electron instabilities, *Gary* [1985] studied two possible modes driven by net relative drift, whistler heat flux instability with plus sign, and electron beam firehose instability with minus sign for isotropic temperatures [see *Gary*, 1985, Table 1]. Here plus and minus designate the sign of cyclotron resonance condition, $\omega \pm \Omega_e = k_\parallel \alpha_\parallel$, where $\Omega_e = eB_0/m_e c$ is the electron gyrofrequency and $\alpha_\parallel$ represents parallel thermal speed. Similarly, under the limit, $\mathbf{k} \times \mathbf{B_0} = 0$, in electromagnetic ion/ion instabilities, for an anisotropic beam in its frame and dynamical plasma betas [*Gary*, 1993], it may possible to consider the self-consistent anisotropy evolution of both plasma and beam ions, as discussed by *Moya et al.* [2011] and *Moya et al.* [2014]. In the present paper, we are interested in perpendicular temperature anisotropy-driven EMEC mode, and for the sake of simplicity, we neglect the net relative drift between core-halo electrons components. We assume zero relative streaming velocity between the two electron populations, following earlier works by *Gary et al.* [1996], *Lazar et al.* [2014], *Shaaban et al.* [2016], and *Lazar et al.* [2016].

In equation (3), $\alpha_{\perp a}$ and $\alpha_{\parallel a}$ stand for perpendicular and parallel thermal speeds for each species, where perpendicular and parallel temperatures are defined by

$$\begin{aligned} T_{\perp a} &= \frac{m_e}{2}\int \mathrm{d}\mathbf{v} v_\perp^2 f_a = \frac{m_e \alpha_{\perp a}^2}{2}, \\ T_{\parallel a} &= m_e \int \mathrm{d}\mathbf{v} v_\parallel^2 f_a = \frac{m_e \alpha_{\parallel a}^2}{2}, \end{aligned} \tag{4}$$

and m_e is the electron mass. The perpendicular and parallel velocity vector components are defined by $v_\perp$ and $v_\parallel$ in cylindrical coordinate. The customary Boltzmann constant is omitted in definition of temperature since we work in centimeter-gram-second (CGS) energy unit for thermal energy.

To reiterate, the above assumed model for electron distribution is, in general, not expected to be valid in a strict sense, but *Seough and Yoon* [2012], *Yoon and Seough* [2012], and *Seough et al.* [2013] successfully adopted such a method to address the related problem of anisotropy-beta inverse relationship for the protons. *Seough et al.* [2014] carried out a comparative study of full particle-in-cell simulation and macroscopic quasi-linear calculation for proton cyclotron instability and showed that the assumption of bi-Maxwellian model for all time and quasi-linear scheme are quite valid. In contrast, *Seough et al.* [2015] showed that the same macroscopic quasi-linear scheme for the proton firehose instability driven by parallel excessive temperature anisotropy did not show good agreement between theory and simulation. The present paper is concerned with perpendicular temperature anisotropy for electrons for which there is no comparative study between simulation and theory, but we will simply extrapolate the findings by *Seough et al.* [2014] and assume that the method is valid.

The adiabatic (or instantaneous) dispersion relation for right-hand circularly polarized electromagnetic electron cyclotron wave is given by

$$\frac{c^2k^2}{\omega^2} = 1 + \sum_{a=i,c,h} \frac{\omega_{pa}^2}{\omega^2} \int \mathrm{d}\mathbf{v}\, \frac{v_\perp/2}{\omega - kv_\parallel + \Omega_a} \left(\left(\omega - kv_\parallel\right) \frac{\partial f_a}{\partial v_\perp} + kv_\perp \frac{\partial f_a}{\partial v_\parallel} \right). \tag{5}$$

In the above, the species label a represents protons ($a = i$), core electrons ($a = c$), and halo electrons ($a = h$). We also consider the parallel propagation of transverse waves, which implies one-dimensional spatial variation along the direction of wave propagation. Employing the adiabatic distribution given in equation (3), the complex frequency and wave number satisfy the following equation:

$$0 = \frac{c^2k^2}{\omega^2} - \frac{\omega_{pi}^2}{\omega k \alpha_i} Z\left(\frac{\omega + \Omega_i}{k\alpha_i}\right) - \sum_{a=c,h} \frac{n_a}{n_0} \frac{\omega_{pe}^2}{\omega^2} \left\{ \frac{T_{\perp a}}{T_{\parallel a}} - 1 + \left[\frac{T_{\perp a}}{T_{\parallel a}}\, \omega - \left(\frac{T_{\perp a}}{T_{\parallel a}} - 1 \right) \Omega_e \right] \frac{1}{k\alpha_{\parallel a}} Z\left(\frac{\omega - \Omega_e}{k\alpha_{\parallel a}} \right) \right\}, \tag{6}$$

where we have ignored the displacement current and assumed isotropic protons, α_i being the proton thermal speed and $T_i = m_i\alpha_i^2/2$ being the proton temperature. In equation (6) the plasma dispersion function is defined by $Z(\zeta) = \int_{-\infty}^{\infty} (x - \zeta)^{-1} e^{-x^2} \mathrm{d}x$, $\omega_{pi} = (4\pi n_0 e^2/m_i)^{1/2}$, $\omega_{pe} = (4\pi n_0 e^2/m_e)^{1/2}$, $\Omega_i = eB_0/m_i c$, and $\Omega_e = eB_0/m_e c$ represent the proton and electron plasma frequencies, and proton and electron cyclotron frequencies, respectively. Here n_0 is the total number density, n_c and n_h are core and halo number densities ($n_0 = n_c + n_h$), B_0 is the ambient magnetic field intensity, e is the unit charge, and c is the speed of light in vacuo. The dispersion relation (6) adiabatically depends upon the time variable t through the temperatures of the electrons.

For the parallel waves and instabilities, the electron kinetic equation in the diffusion approximation, taking into account only the right-hand polarized mode, is

$$\begin{aligned} \frac{\partial f_a}{\partial t} = {} & \frac{ie^2}{4m_e^2c^2} \frac{1}{v_\perp} \int_{-\infty}^{\infty} \frac{\mathrm{d}k}{k^2} \left[\left(\omega^* - kv_\parallel\right) \frac{\partial}{\partial v_\perp} + kv_\perp \frac{\partial}{\partial v_\parallel} \right] \\ & \times \frac{v_\perp \delta B^2(k,\omega)}{\omega - kv_\parallel + \Omega_a} \left[\left(\omega - kv_\parallel\right) \frac{\partial f_a}{\partial v_\perp} + kv_\perp \frac{\partial f_a}{\partial v_\parallel} \right], \end{aligned} \tag{7}$$

where $a = c, h$, $\omega = \omega_k + i\gamma_k$ is the complex root of equation (6) and $\delta B^2(k)$ is the spectral wave energy density associated with electromagnetic cyclotron mode magnetic field perturbations. Taking the appropriate moments of the above equation, we obtain

$$\begin{aligned} \frac{\mathrm{d}T_{\perp a}}{\mathrm{d}t} &= -\frac{e^2}{2m_e c^2} \int_{-\infty}^{\infty} \frac{\mathrm{d}k}{k^2}\, \delta B^2(k) \left\{ \left(\frac{2T_{\perp a}}{T_{\parallel a}} - 1 \right) \gamma_k + \mathrm{Im}\, \frac{2i\gamma - \Omega_e}{k\alpha_{\parallel a}} \left[\frac{T_{\perp a}}{T_{\parallel a}}\, \omega - \left(\frac{T_{\perp a}}{T_{\parallel a}} - 1 \right) \Omega_e \right] Z\left(\frac{\omega - \Omega_e}{k\alpha_{\parallel a}} \right) \right\}, \\ \frac{\mathrm{d}T_{\parallel a}}{\mathrm{d}t} &= \frac{e^2}{m_e c^2} \int_{-\infty}^{\infty} \frac{\mathrm{d}k}{k^2}\, \delta B^2(k) \left\{ \frac{T_{\perp a}}{T_{\parallel a}}\, \gamma_k + \mathrm{Im}\, \frac{\omega - \Omega_e}{k\alpha_{\parallel a}} \left[\frac{T_{\perp a}}{T_{\parallel a}}\, \omega - \left(\frac{T_{\perp a}}{T_{\parallel a}} - 1 \right) \Omega_e \right] Z\left(\frac{\omega - \Omega_e}{k\alpha_{\parallel a}} \right) \right\}, \end{aligned} \tag{8}$$

where $a = c, h$. The wave kinetic equation is given by

$$\frac{\partial \delta B^2(k)}{\partial t} = 2\gamma_k\, \delta B^2(k). \tag{9}$$

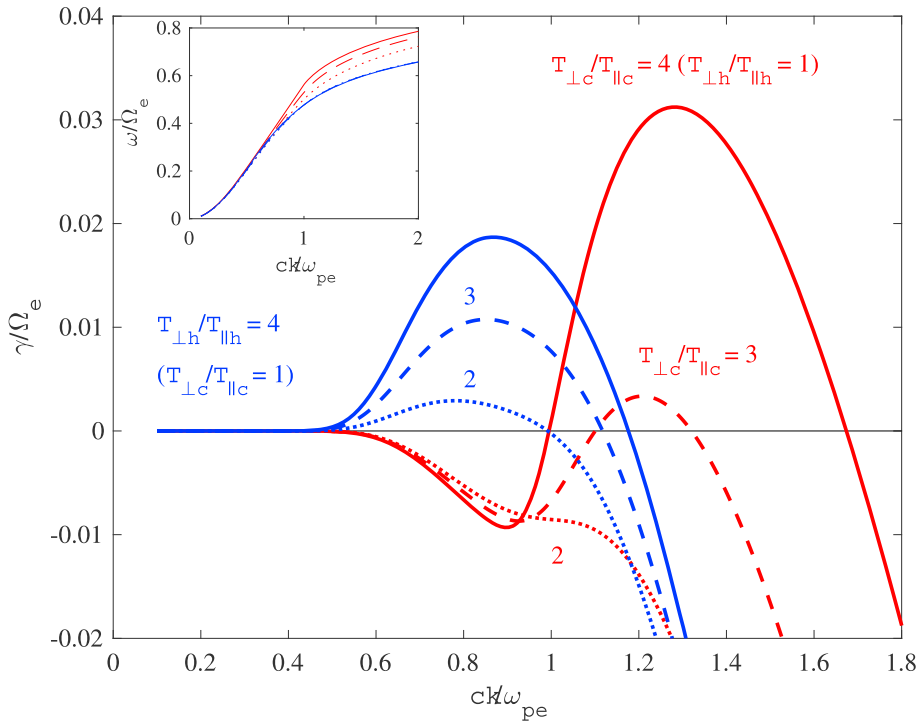

Figure 1. Complex real frequency ω_k/Ω_e (inset) and growth rate γ_k/Ω_e versus normalized wave number, ck/ω_{pe}, for different combinations of temperature ratios for core and halo electrons. The case of isotropic core and anisotropic halo (cases A, B, and C) is shown with blue curves (with each halo anisotropy indicated by solid, dashed, and dotted curves). The labels are also indicated with the same blue text color for the ease of visual inspection. The opposite case of isotropic halo and anisotropic core (cases D, E, and F) is plotted with red curve. For detailed input parameters, refer to the text.

3. Numerical Analysis

For numerical analysis, we introduce the following dimensionless quantities associated with normalized frequency, z (normalized to electron gyrofrequency), and normalized wave number, q (normalized to electron skin depth); halo electron density ratio, δ, and proton-to-electron mass ratio, M; Z function arguments for ions (protons), ξ_i and ζ_i, as well as ion beta; core and halo electron Z function arguments, ζ_c and ζ_h, as well as quantities η_c and η_h; and core and halo anisotropy factors, A_c and A_h, as well as their parallel betas, β_c and β_h; normalized time, τ (normalized to inverse electron gyroperiod), and normalized magnetic field wave energy density, $W(q)$ (normalized to ambient magnetic field energy density):

$$
\begin{aligned}
&z = \frac{\omega}{\Omega_e}, \quad q = \frac{ck}{\omega_{pe}}, \quad \delta = \frac{n_h}{n_0}, \quad M = \frac{m_i}{m_e},\\
&\xi_i = \frac{z}{q(M\beta_i)^{1/2}}, \quad \zeta_i = \frac{Mz+1}{q(M\beta_i)^{1/2}}, \quad \beta_i = \frac{8\pi n_0 T_i}{B_0^2},\\
&\zeta_c = \frac{z-1}{q\beta_c^{1/2}}, \quad \eta_c = \frac{(A_c+1)z - A_c}{q\beta_{\|c}^{1/2}},\\
&A_c = \frac{\beta_{\perp c}}{\beta_{\|c}} - 1, \quad \beta_c = \frac{8\pi n_0 T_{\|c}}{B_0^2},\\
&\zeta_h = \frac{z-1}{q\beta_h^{1/2}}, \quad \eta_h = \frac{(A_h+1)z - A_h}{q\beta_{\|h}^{1/2}},\\
&A_h = \frac{\beta_{\perp h}}{\beta_{\|h}} - 1, \quad \beta_h = \frac{8\pi n_0 T_{\|h}}{B_0^2},\\
&\tau = \Omega_e t, \quad W(q) = \frac{\delta B^2(q)}{B_0^2}.
\end{aligned}
\tag{10}
$$

Let us rewrite equations (6), (8), and (9) in normalized form as

$$0 = q^2 - \xi_i Z(\zeta_i) - (1-\delta)\left[A_c + \eta_c Z(\zeta_c)\right] - \delta\left[A_h + \eta_h Z(\zeta_h)\right], \tag{11}$$

$$\begin{aligned}
\frac{\mathrm{d}\beta_{\perp c}}{\mathrm{d}\tau} &= -2\int_0^\infty \mathrm{d}q\,\frac{W(q)}{q^2}\left[\left(2A_c+1\right)z_i + \mathrm{Im}\left(2iz_i - 1\right)\eta_c Z(\zeta_c)\right],\\
\frac{\mathrm{d}\beta_{\parallel c}}{\mathrm{d}\tau} &= 4\int_0^\infty \mathrm{d}q\,\frac{W(q)}{q^2}\left[\left(A_c+1\right)z_i + \mathrm{Im}\left(z-1\right)\eta_c Z(\zeta_c)\right],\\
\frac{\mathrm{d}\beta_{\perp h}}{d\tau} &= -2\int_0^\infty \mathrm{d}q\,\frac{W(q)}{q^2}\left[\left(2A_h+1\right)z_i + \mathrm{Im}\left(2iz_i - 1\right)\eta_h Z(\zeta_h)\right],\\
\frac{\mathrm{d}\beta_{\parallel h}}{\mathrm{d}\tau} &= 4\int_0^\infty \mathrm{d}q\,\frac{W(q)}{q^2}\left[\left(A_h+1\right)z_i + \mathrm{Im}\left(z-1\right)\eta_h Z(\zeta_h)\right],
\end{aligned} \tag{12}$$

$$\frac{\partial W(q)}{\partial \tau} = 2z_i W(q). \tag{13}$$

Note that the dispersion relation is not only a function normalized frequency z and normalized wave number q, but it also depends implicitly upon seven dimensionless input parameters, δ, M, β_i, β_c, β_h, A_c, and A_h.

Numerical solutions to equation (11) are presented in Figure 1. For this graphical analysis, realistic values of parameters $n_c/n_0 = 1-\delta = 0.95$, $\delta = n_h/n_0 = 0.05$, $\beta_i = 0.04 = \beta_c$, and $\beta_h = 0.36$ have been used. Figure 1 shows the variation of normalized frequency, $z_r = \omega_k/\Omega_e$, growth rate, $z_i = \gamma_k/\Omega_e$, against the wave number, $q = ck/\omega_{pe}$, for different anisotropic ratios of core and halo components, namely,

$$\begin{aligned}
\text{Case A:}\quad & \left(\frac{T_{\perp c}}{T_{\parallel c}}, \beta_c\right) = (1, 0.04), \left(\frac{T_{\perp h}}{T_{\parallel h}}, \beta_h\right) = (4, 0.36),\\
\text{Case B:}\quad & \left(\frac{T_{\perp c}}{T_{\parallel c}}, \beta_c\right) = (1, 0.04), \left(\frac{T_{\perp h}}{T_{\parallel h}}, \beta_h\right) = (3, 0.36),\\
\text{Case C:}\quad & \left(\frac{T_{\perp c}}{T_{\parallel c}}, \beta_c\right) = (1, 0.04), \left(\frac{T_{\perp h}}{T_{\parallel h}}, \beta_h\right) = (2, 0.36),\\
\text{Case D:}\quad & \left(\frac{T_{\perp h}}{T_{\parallel h}}, \beta_h\right) = (1, 0.36), \left(\frac{T_{\perp c}}{T_{\parallel c}}, \beta_c\right) = (4, 0.04),\\
\text{Case E:}\quad & \left(\frac{T_{\perp h}}{T_{\parallel h}}, \beta_h\right) = (1, 0.36), \left(\frac{T_{\perp c}}{T_{\parallel c}}, \beta_c\right) = (3, 0.04),\\
\text{Case F:}\quad & \left(\frac{T_{\perp h}}{T_{\parallel h}}, \beta_h\right) = (1, 0.36), \left(\frac{T_{\perp c}}{T_{\parallel c}}, \beta_c\right) = (2, 0.04).
\end{aligned}$$

First three cases show the influence of halo anisotropy variation while keeping the core component as isotropic (the choice of parameters is based observations), while in the second set of three cases, we investigate the effect of variation in the core anisotropy by taking halo as isotropic (which is rarely observed, but we consider such combinations for the sake of pedagogy). Observe that for constant halo temperature ratio, the real frequency increases for increasing core temperature ratio, but when the core is isotropic the real frequency appears independent of the change in halo temperature ratio. Notice that core anisotropy leads to higher growth rate. This is because the core with higher density has more thermal energy. Note also that the range of unstable modes depends on the free energy source, that is, core versus halo anisotropy.

In subsequent numerical analysis of quasi-linear evolution of EMEC instability, we restrict ourselves to $k > 0$ integral domain and simply multiply factor 2 to right-hand side of equation (12). For quasi-linear analysis, we extend the number of cases up to nine combinations of input parameters. Note that the linear stability analysis presented in Figure 1 was to showcase the influence of each anisotropic component, but the subsequent quasi-linear analysis is not exactly the same as that of Figure 1. Indeed, it does not have to be, and for quasi-linear analysis, we generally consider different combinations of core-halo anisotropies as suggested in Table 1 of *Lazar et al.* [2014]. We go beyond their linear analysis to discuss the time evolution and to evaluate the asymptotic excitation and saturation of EMEC instability. Figure 2 depicts the time history of variation in

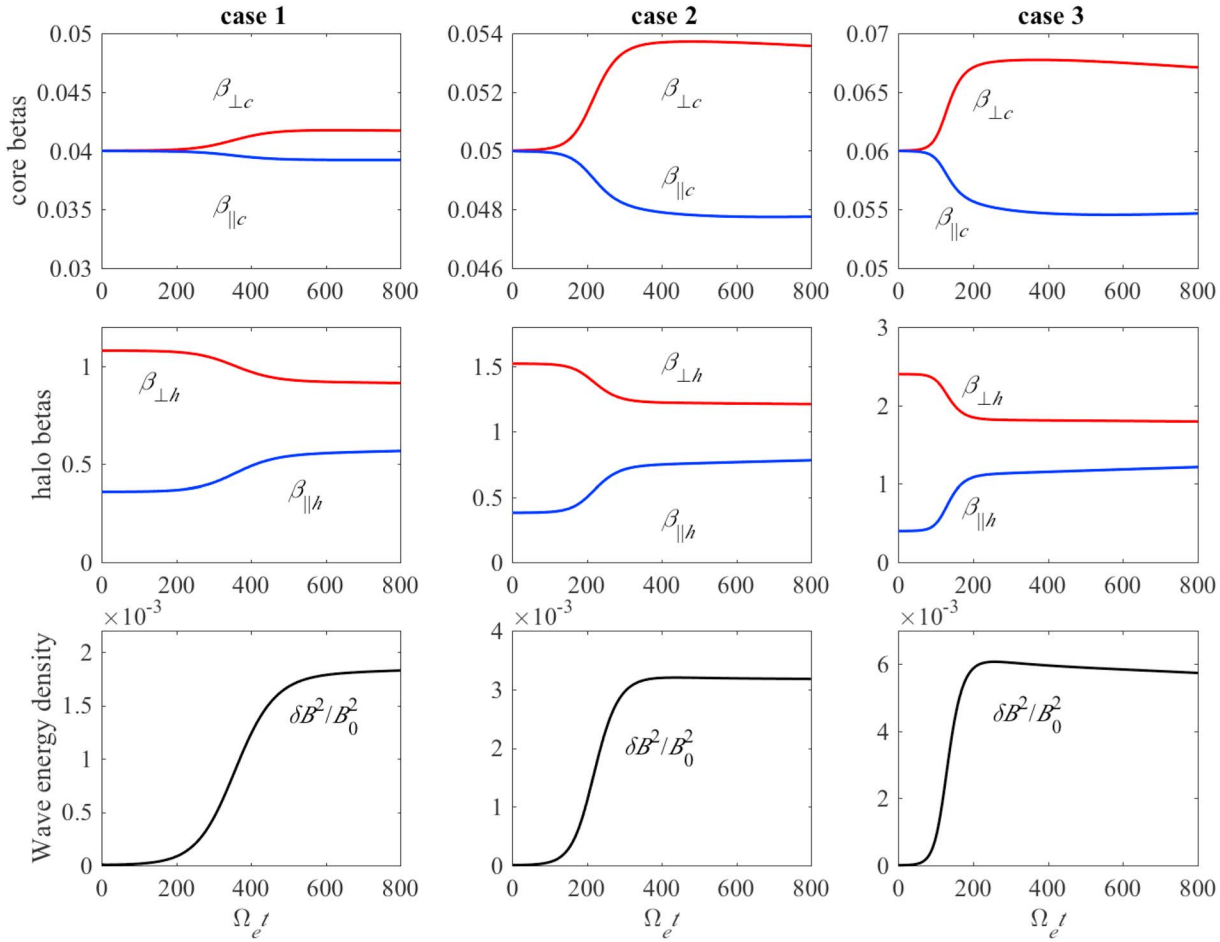

Figure 2. Time evolution of normalized temperatures (betas) for (top row) core component, $\beta_{\perp c}$ and $\beta_{\parallel c}$, for (middle row) halo component, $\beta_{\perp h}$ and $\beta_{\parallel h}$, and (bottom row) wave energy density $\delta B^2/B_0^2$, versus normalized time, $\tau = \Omega_e t$, for initially isotropic core electrons component. (left column) For initial halo anisotropy $\beta_{\perp h}(0)/\beta_{\parallel h}(0) = 3$, $\beta_{\parallel h}(0) = 0.36$, and $\beta_{\perp c}(0) = \beta_{\parallel c}(0) = 0.04$; (middle column) for $\beta_{\perp h}(0)/\beta_{\parallel h}(0) = 4$, $\beta_{\parallel h}(0) = 0.38$, and $\beta_{\perp c}(0) = \beta_{\parallel c}(0) = 0.05$; (right column) the initial condition $\beta_{\perp h}(0)/\beta_{\parallel h}(0) = 6$, $\beta_{\parallel h}(0) = 0.40$, and $\beta_{\perp c}(0) = \beta_{\parallel c}(0) = 0.06$.

normalized temperatures (or betas) for core and halo electrons and wave energy density. The initial conditions are chosen as various combinations of the following parameters:

$$
\begin{aligned}
& W(k) = 10^{-6}, \\
\text{Case 1:}\quad & \frac{T_{\perp c}(0)}{T_{\parallel c}(0)} = \frac{\beta_{\perp c}(0)}{\beta_{\parallel c}(0)} = 1, \quad \beta_{\parallel c}(0) = 0.04, \\
& \frac{T_{\perp h}(0)}{T_{\parallel h}(0)} = \frac{\beta_{\perp h}(0)}{\beta_{\parallel h}(0)} = 3, \quad \beta_{\parallel h}(0) = 0.36, \\
\text{Case 2:}\quad & \frac{T_{\perp c}(0)}{T_{\parallel c}(0)} = \frac{\beta_{\perp c}(0)}{\beta_{\parallel c}(0)} = 1, \quad \beta_{\parallel c}(0) = 0.05, \\
& \frac{T_{\perp h}(0)}{T_{\parallel h}(0)} = \frac{\beta_{\perp h}(0)}{\beta_{\parallel h}(0)} = 4, \quad \beta_{\parallel h}(0) = 0.38, \\
\text{Case 3:}\quad & \frac{T_{\perp c}(0)}{T_{\parallel c}(0)} = \frac{\beta_{\perp c}(0)}{\beta_{\parallel c}(0)} = 1, \quad \beta_{\parallel c}(0) = 0.06, \\
& \frac{T_{\perp h}(0)}{T_{\parallel h}(0)} = \frac{\beta_{\perp h}(0)}{\beta_{\parallel h}(0)} = 6, \quad \beta_{\parallel h}(0) = 0.40.
\end{aligned}
\tag{14}
$$

Figure 2 (left column) is for initial values of $T_{\perp h}(0)/T_{\parallel h}(0) = 3$, $\beta_{\parallel h}(0) = 0.36$, and $\beta_{\perp c}(0) = \beta_{\parallel c}(0) = 0.04$; Figure 2 (middle column) is for $T_{\perp h}(0)/T_{\parallel h}(0) = 4$, $\beta_{\parallel h}(0) = 0.38$, and $\beta_{\perp c}(0) = \beta_{\parallel c}(0) = 0.05$; Figure 2 (right column) is for $T_{\perp h}(0)/T_{\parallel h}(0) = 6$, $\beta_{\parallel h}(0) = 0.40$, and $\beta_{\perp c}(0) = \beta_{\parallel c}(0) = 0.06$. Figure 2 thus shows three different

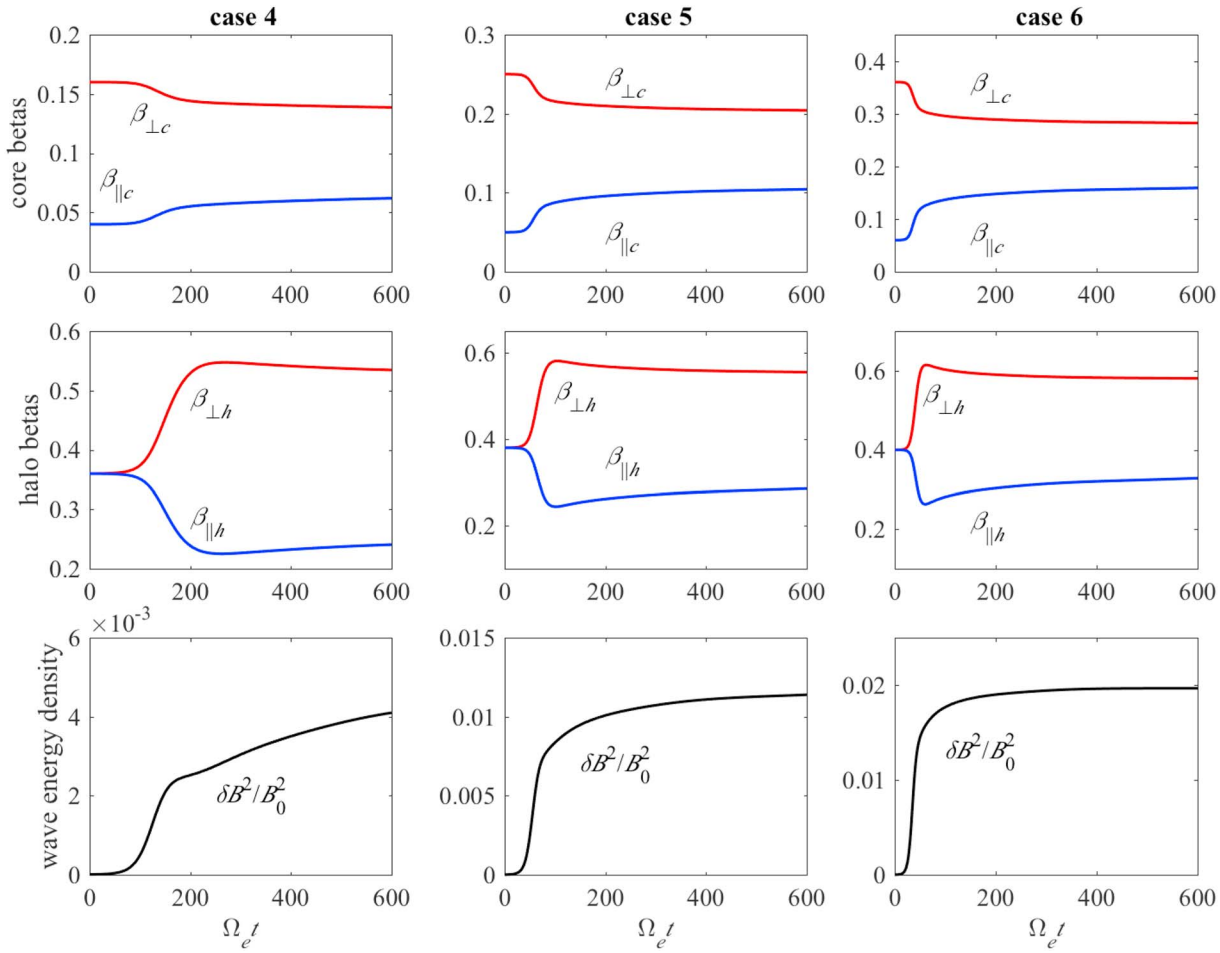

Figure 3. The same as Figure 2 except that we consider initially isotropic halo electrons. (left column) Initial core anisotropy $\beta_{\perp c}(0)/\beta_{\parallel c}(0) = 4$, $\beta_{\parallel c}(0) = 0.04$, and $\beta_{\perp h}(0) = \beta_{\parallel h}(0) = 0.36$; (middle column) $\beta_{\perp c}(0)/\beta_{\parallel c}(0) = 5$, $\beta_{\parallel h}(0) = 0.05$, and $\beta_{\perp h}(0) = \beta_{\parallel h}(0) = 0.38$; (right column) The initial condition $\beta_{\perp c}(0)/\beta_{\parallel c}(0) = 6$, $\beta_{\parallel h}(0) = 0.06$, and $\beta_{\perp h}(0) = \beta_{\parallel h}(0) = 0.4$.

cases in which the core electron component is initially isotropic. Such combinations of initial parameters can be regarded as more typical of the solar wind. As EMEC instability is excited and develops in time, however, it can be seen that the core anisotropy spontaneously develops such that the initial isotropy is not maintained. In all three cases, it is interesting to note that the core electrons undergo slight perpendicular heating, while the parallel temperature generally decreases from the initial value (except in the first case–Figure 2 (left column, top), where the core parallel beta first decreases then undergoes increase again). In the case of Figure 2, the free energy for EMEC instability is provided by the halo electron temperature anisotropy. Initially, the wave density increases exponentially in agreement with linear theory. As the time passes, the rise in wave amplitude is constrained at the quasi-linear stage of time evolution and amplitude of the wave saturates at its maximum value in the first two cases (Figure 2, left and middle columns). However, in the third case there the temperature anisotropy is the highest, the wave energy first exponentially grows, followed by quasi-saturation, but beyond the saturation stage, the wave energy gradually decreases as a result of reabsorption of the wave energy by the electrons. The perpendicular temperature of halo electrons generally decreases as the free energy is transferred to EMEC waves, which in turn heats the halo electrons in parallel direction, thus reducing the initial anisotropy. Note that for higher initial halo temperature anisotropy, the instability onset time becomes progressively earlier, and the quasi-linear saturation also occurs earlier for higher temperature anisotropy. This is, of course, easy to understand since higher anisotropy means more available free energy, and thus, the instability growth rate is higher.

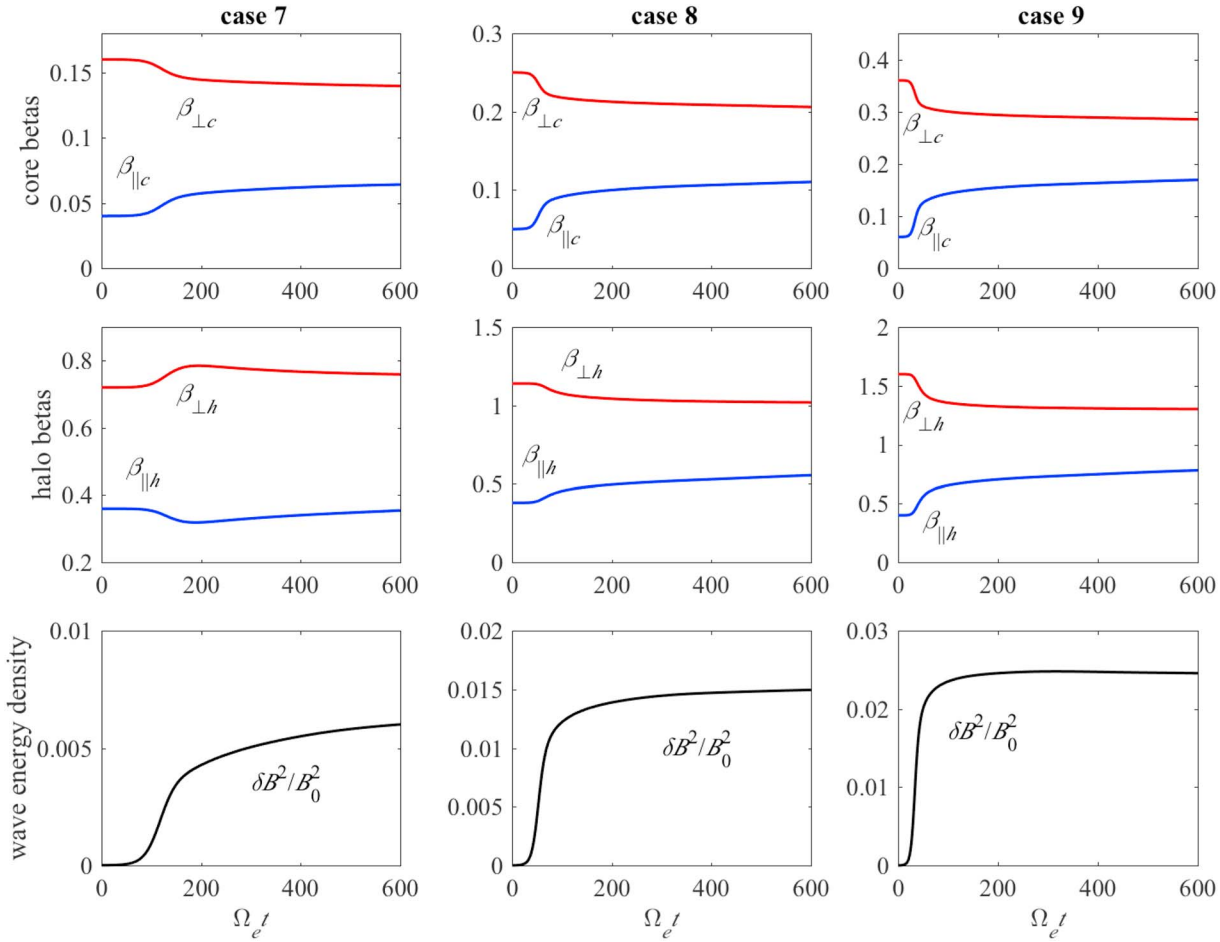

Figure 4. The same as Figure 2 except that we consider initially isotropic halo electrons. (left column) Initial core anisotropy $\beta_{\perp c}(0)/\beta_{\|c}(0) = 4$, $\beta_{\|c}(0) = 0.04$, and $\beta_{\perp h}(0)/\beta_{\|h}(0) = 2$, $\beta_{\|h}(0) = 0.36$; (middle column) $\beta_{\perp c}(0)/\beta_{\|c}(0) = 5$, $\beta_{\|h}(0) = 0.05$, and $\beta_{\perp h}(0)/\beta_{\|h}(0) = 3$, $\beta_{\|h}(0) = 0.38$; (right column) initial condition $\beta_{\perp c}(0)/\beta_{\|c}(0) = 6$, $\beta_{\|h}(0) = 0.06$, and $\beta_{\perp h}(0)/\beta_{\|h}(0) = 4$, $\beta_{\|h}(0) = 0.4$.

Figure 3 display numerical solutions in which the initial conditions are $W(k) = 10^{-6}$ and

$$
\begin{aligned}
\text{Case 4:}\quad & \frac{T_{\perp c}(0)}{T_{\|c}(0)} = \frac{\beta_{\perp c}(0)}{\beta_{\|c}(0)} = 4, \quad \beta_{\|c}(0) = 0.04,\\
& \frac{T_{\perp h}(0)}{T_{\|h}(0)} = \frac{\beta_{\perp h}(0)}{\beta_{\|h}(0)} = 1, \quad \beta_{\|h}(0) = 0.36,\\
\text{Case 5:}\quad & \frac{T_{\perp c}(0)}{T_{\|c}(0)} = \frac{\beta_{\perp c}(0)}{\beta_{\|c}(0)} = 5, \quad \beta_{\|c}(0) = 0.05,\\
& \frac{T_{\perp h}(0)}{T_{\|h}(0)} = \frac{\beta_{\perp h}(0)}{\beta_{\|h}(0)} = 1, \quad \beta_{\|h}(0) = 0.38,\\
\text{Case 6:}\quad & \frac{T_{\perp c}(0)}{T_{\|c}(0)} = \frac{\beta_{\perp c}(0)}{\beta_{\|c}(0)} = 6, \quad \beta_{\|c}(0) = 0.06,\\
& \frac{T_{\perp h}(0)}{T_{\|h}(0)} = \frac{\beta_{\perp h}(0)}{\beta_{\|h}(0)} = 1, \quad \beta_{\|h}(0) = 0.40.
\end{aligned}
\tag{15}
$$

Thus, for Figure 3, we hold the halo electrons to be isotropic but consider initially anisotropic core electrons, which is, in fact, a rare combination of anisotropies to be observed in solar wind environment. Nevertheless, we consider such initial conditions for the sake of pedagogy and completeness. Figure 3 (left column) is for initial values of $T_{\perp c}(0)/T_{\|c}(0) = 4$, $\beta_{\|h}(0) = 0.04$, and $\beta_{\perp h}(0) = \beta_{\|h}(0) = 0.36$; the initial condition for Figure 3 (middle column) corresponds to $T_{\perp c}(0)/T_{\|c}(0) = 5$, $\beta_{\|h}(0) = 0.05$, and $\beta_{\perp h}(0) = \beta_{\|h}(0) = 0.38$; and Figure 3 (right column) is for $T_{\perp c}(0)/T_{\|c}(0) = 6$, $\beta_{\|h}(0) = 0.06$, and $\beta_{\perp h}(0) = \beta_{\|h}(0) = 0.4$. Figure 3 demonstrates the

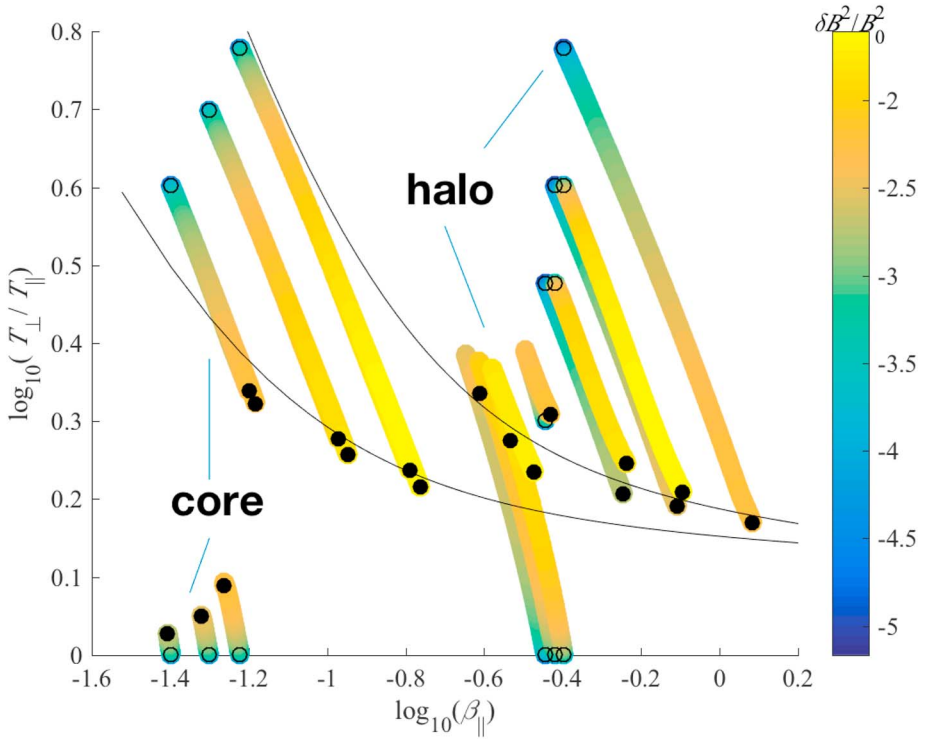

Figure 5. Dynamical paths of all nine cases considered in Figures 2–4. The evolutionary paths of core temperatures and halo temperatures are plotted with magnetic field intensity color coded along the paths. Initial positions in $(T_\perp/T_\parallel, \beta_\parallel)$ phase space are indicated by open circles, while the final positions are marked with large dots. We have also superposed two heuristic marginal stability curves following *Lazar et al.* [2015].

time evolution of temperature anisotropies of core and halo populations along with wave energy density. Just as with Figure 2, it can be inferred from the figure that the initially higher values of parallel betas and temperature anisotropies trigger the EMEC mode to get excited more rapidly and saturate early. The trend of increasing wave energy density is also similar with the previous case, except that in the present, we do not observe slow reabsorption of wave energy. The initially isotropic halo electrons are seen to be heated in perpendicular direction while undergoing parallel cooling. This is consistent with those shown Figure 2. The initially anisotropic core electrons also evolve in a similar manner as before in that the anisotropy is reduced as a result of reduction of perpendicular core temperature and an increase in the parallel core temperature.

In Figure 4, we now consider the case when both core and halo possess initial anisotropies, which is more typical of the solar wind as discussed by many previous observational papers. Specifically, the following initial conditions are employed ($W(k) = 10^{-6}$ as in other cases):

$$\begin{aligned}
\text{Case 7:}\quad & \frac{T_{\perp c}(0)}{T_{\parallel c}(0)} = \frac{\beta_{\perp c}(0)}{\beta_{\parallel c}(0)} = 4, \quad \beta_{\parallel c}(0) = 0.04,\\
& \frac{T_{\perp h}(0)}{T_{\parallel h}(0)} = \frac{\beta_{\perp h}(0)}{\beta_{\parallel h}(0)} = 2, \quad \beta_{\parallel h}(0) = 0.36,\\
\text{Case 8:}\quad & \frac{T_{\perp c}(0)}{T_{\parallel c}(0)} = \frac{\beta_{\perp c}(0)}{\beta_{\parallel c}(0)} = 5, \quad \beta_{\parallel c}(0) = 0.05,\\
& \frac{T_{\perp h}(0)}{T_{\parallel h}(0)} = \frac{\beta_{\perp h}(0)}{\beta_{\parallel h}(0)} = 3, \quad \beta_{\parallel h}(0) = 0.38,\\
\text{Case 9:}\quad & \frac{T_{\perp c}(0)}{T_{\parallel c}(0)} = \frac{\beta_{\perp c}(0)}{\beta_{\parallel c}(0)} = 6, \quad \beta_{\parallel c}(0) = 0.06,\\
& \frac{T_{\perp h}(0)}{T_{\parallel h}(0)} = \frac{\beta_{\perp h}(0)}{\beta_{\parallel h}(0)} = 4, \quad \beta_{\parallel h}(0) = 0.40.
\end{aligned} \tag{16}$$

Figure 4 (left column) is for initial values $\beta_{\perp c}(0)/\beta_{\parallel c}(0) = 4$, $\beta_{\parallel c}(0) = 0.04$, and $\beta_{\perp h}(0)/\beta_{\parallel h}(0) = 2$, $\beta_{\parallel h}(0) = 0.36$; the initial condition for Figure 4 (middle column) corresponds to $\beta_{\perp c}(0)/\beta_{\parallel c}(0) = 5$, $\beta_{\parallel h}(0) = 0.05$, and

$\beta_{\perp h}(0)/\beta_{\parallel h}(0) = 3$, $\beta_{\parallel h}(0) = 0.38$; and Figure 4 (right column) is for $\beta_{\perp c}(0)/\beta_{\parallel c}(0) = 6$, $\beta_{\parallel h}(0) = 0.06$, and $\beta_{\perp h}(0)/\beta_{\parallel h}(0) = 4, \beta_{\parallel h}(0) = 0.4$. In this case, both electron species provide the free energy for the wave growth, but since the core is the dominant species, the EMEC growth is determined by the core. Figure 4 shows that the perpendicular betas for core electrons undergo reduction, while the parallel betas increase, implying that the wave excitation takes place at the expense of the core-free energy. In contrast, the halo electrons exhibit time evolution that could not have been predicted by linear theory. In the first case (Figure 4, left column) of relatively low halo anisotropy, the halo electrons simply undergo mild perpendicular heating and parallel cooling, much like that of Figure 3. However, subsequently, the halo anisotropy is increased (middle). It can be seen that the initial halo perpendicular beta gradually decreases while concomitantly, the initial halo beta increases. This is an indication that the halo electrons also participate in the wave energy production. Finally, Figure 4 (right column), which corresponds to the highest halo anisotropy among the three cases considered, one can see that the halo anisotropy reduction and general evolution of halo temperatures (or betas) are qualitatively similar to that of the core. This is evidence that both core and halo populations contribute to the EMEC instability process.

In Figure 5, we replot the results shown in Figures 2–4 in a different way. We combine all nine cases into a single plot by following the dynamic paths of each cases. We plot the core and halo temperatures as paths in $(T_\perp/T_\parallel, \beta_\parallel)$ phase space, but we also color code the strength of the magnetic field using color scale. Consequently, Figure 5 has both particle and field information for all the cases considered, so far. We also superpose the empirical marginal stability curves for core-driven EMEC instability and halo-driven EMEC instability by making use of *Lazar et al.*, 2015's [2015] formula. In relation to observational data, it is possible to display the instability threshold analysis for anisotropic core and halo electrons components separately [see *Štverák et al.*, 2008, Figures 5 and 6]. Here we have an improved formula (equation (2)) to show the core-driven and halo-driven instability thresholds. For core electrons, *Štverák et al.* [2008] suggested a better agreement of linear theory prediction and observed data results obtained in thermal core population. Following the same idea, we employed the fitting parameters given in Table A1 of *Lazar et al.* [2015] in thermal core column (T) under limit $\kappa \to \infty$. For $\gamma_{\max}/\Omega_e = 10^{-2}$ and $n_h/n_c = 0.05$, equation (2) takes the form as

$$\frac{T_{\perp c}}{T_{\parallel c}} = 1 + \frac{0.4}{\beta_{\parallel c}^{0.1}}\left(1 + \frac{0.05}{\beta_{\parallel c}^{1.26}}\right). \tag{17}$$

The above fit corresponds to the bottom curve, and it describes the asymptotic state of the initially unstable core electron parameters. The second fitting formula is essentially the same as equation (2) in form, except that the parameters a, b, c, and d are different. Specifically,

$$\frac{T_{\perp h}}{T_{\parallel h}} = 1 + \frac{0.5}{\beta_{\parallel h}^{0.2}}\left(1 + \frac{0.08}{\beta_{\parallel h}^{1.5}}\right). \tag{18}$$

The above formula appears to fit the asymptotic states of halo electrons, and it corresponds to the upper curve.

4. Summary and Discussion

The radially expanding solar wind plasma has remained a subject of considerable interest for many years. In the literature, the electrons in the solar wind are modeled by different combinations of distributions with the aid of available data from different spacecraft. Observed data suggest the presence of two populations of electrons in the solar wind. The proposed distribution function is composed of a highly dense core along with less dense and highly energetic halo component of electrons. Observations also show that both core and halo electrons can exhibit temperature anisotropies. For excessive perpendicular temperature anisotropy for these electrons it is known that electromagnetic electron cyclotron (EMEC) instability can be excited, while for excessive parallel temperature anisotropy, electron firehose instability may be excited. The present paper is concerned with the former, namely, EMEC instability excitation and evolution.

In the present paper, considering realistic parameters, we assumed both core and halo components as bi-Maxwellian. While we assumed the basic bi-Maxwellian form in mathematical sense, we allowed the temperature of these populations to vary in time t. By employing such a model, we performed quasi-linear analysis

of the temperature anisotropy-driven EMEC instability when the free energy source (i.e., the temperature anisotropy) is provided by either the core or the halo (and also, we considered when both are anisotropic as well). The justification for the present approximation is that we are concerned with bulk properties of plasma, i.e., the moments of the distribution function.

Figures 2–4 show in detail several different combinations of initial conditions. When the instability driven by the temperature anisotropy of one population while the other component is initially assumed isotropic, we found that the isotropic component does not stay isotropic during the instability development, but rather, the evolution is characterized by perpendicular heating and parallel cooling. When both populations are anisotropic, then the time development of the instability becomes a bit more complicated in that sometimes one species simply responds to the excitation of EMEC instability, but in other cases, both unstable population participate in the instability development. The present instability threshold analysis of EMEC instability via quasi-linear approach is based upon observational spacecraft data as reported by *Pilipp et al.* [1987], *Maksimovic et al.* [2005], *Štverák et al.* [2008], and *Štverák et al.* [2009].

Many authors discussed marginal stability conditions by employing linear growth rate analysis and empirically fitting the marginal growth rate. Such efforts are often plotted as the anisotropy-beta inverse relationship. In the present quasi-linear analysis, we have demonstrated that the marginal stability condition automatically corresponds to the saturation stage of the quasi-linear instability development process; hence, our results are consistent with the empirical threshold conditions. Moreover, it is shown that the present macroscopic quasi-linear analysis is able to compute the saturated wave magnetic field intensity level as a function of the temperature ratio (for either core or halo) and parallel betas.

Similar analysis involving parallel electron firehose can be carried out, which is a subject of future work. Another future task is to extend the analysis to inhomogeneous medium [*Yoon and Seough*, 2014]. Furthermore, instabilities excited in fundamentally two- (or three) dimensional space, such as the oblique electron firehose instability [*Li and Habbal*, 2000] should be considered within the present macroscopic quasi-linear framework. Finally, the method itself, namely, assuming simple distribution functions and employing macroscopic quasi-linear analysis, should be validated by comparing against full particle simulations. These are subjects for future researches.

Finally, it should be noted that although the strahl density is quite low (~about 1–2% of the total density), the differential streaming velocity along the field lines, which can be much higher than the core thermal speed, makes the strahl a potentially important contributor to not only the heat flux but also effective parallel temperature. The present analysis only considered thermal anisotropies owing to the core-halo thermal effects, but the streaming effects by the strahl may be particularly important for electron firehose instability analysis.

Acknowledgments

The present paper does not involve any spacecraft data analysis. However, upon request, numerical data for generating all the figures will be made available. M.S. and S.S. acknowledge support from Higher Education Commission (HEC), Pakistan. P.H.Y. acknowledges NSF grant AGS1550566 to the University of Maryland and the BK21 plus program from the National Research Foundation (NRF), Korea, to Kyung Hee University. He also acknowledges the Science Award Grant from the GFT Foundation to the University of Maryland.

References

Bruno, R. (2013), The solar wind as a turbulence laboratory, *Living Rev. Sol. Phys.*, *10*, 2, doi:10.12942/lrsp-2013-2.

Chew, G. F., M. L. Goldberger, and F. E. Low (1956), The Boltzmann equation and the one-fluid hydromagnetic equations in the absence of particle collisions, *Proc. R. Soc. London. Sr. A*, *236*, 112–118, doi:10.1098/rspa.1956.0116.

Davidson, R. C., and J. M. Ogden (1975), Electromagnetic ion cyclotron instability driven by ion energy anisotropy in high beta plasmas, *Phys. Fluids*, *18*, 1045–1050, doi:10.1063/1.861253.

Dum, C. T., E. Marsch, and W. Pilipp (1980), Determination of wave growth from measured distribution functions and transport theory, *J. Plasma Phys.*, *23*, 91–113, doi:10.1017/S0022377800022170.

Eliasson, B., and M. Lazar (2015), Nonlinear evolution of the electromagnetic electron-cyclotron instability in a bi-Kappa distributed plasma, *Phys. Plasmas*, *22*, 062109, doi:10.1063/1.4922479.

Feldman, W. C., J. R. Asbridge, S. J. Bame, M. D. Montgomery, and S. P. Gary (1975), Solar wind electrons, *J. Geophys. Res.*, *80*, 4181–4196, doi:10.1029/JA080i031p04181.

Gary, S. P., W. C. Feldman, D. W. Forslund, and M. D. Montgomery (1975), Electron heat flux instabilities in the solar wind, *Geophys. Res. Lett.*, *2*, 79–82, doi:10.1029/GL002i003p00079.

Gary, S. P., and W. C. Feldman (1977), Solar wind heat flux regulation by the whistler instability, *J. Geophys. Res.*, *82*, 1087–1094, doi:10.1029/JA082i007p01087.

Gary, S. P. (1985), Electromagnetic electron beam instabilities: Hot, isotropic beams, *J. Geophys. Res.*, *90*, 10,815–10,822, doi:10.1029/JA090iA11p10815.

Gary, S. P. (1993), *Theory of Space Plasma Microinstabilities*, Cambridge Univ. Press, Cambridge.

Gary, S. P., E. E. Scime, J. L. Phillips, and W. C. Feldman (1994), The whistler heat flux instability: Threshold conditions in the solar wind, *J. Geophys. Res.*, *99*, 23,391–23,399, doi:10.1029/94JA02067.

Gary, S. P., and J. Wang (1996), Whistler instability: Electron anisotropy upper bound, *J. Geophys. Res.*, *101*, 10,749–10,754, doi:10.1029/96JA00323.

Gary, S. P., V. M. Vazquez, and D. Winske (1996), Electromagnetic proton cyclotron instability: Proton velocity distributions, *J. Geophys. Res.*, *101*, 13,327–13,333, doi:10.1029/96JA00295.

Gary, S. P., and K. Nishimura (2003), Resonant electron firehose instability: Particle-in-cell simulations, *Phys. Plasmas*, *10*, 3571, doi:10.1063/1.1590982.
Goldstein, M. L., et al. (2015), Multipoint observations of plasma phenomena made in space by Cluster, *J. Plasma Phys.*, *82*, 325810301, doi:10.1017/S0022377815000185.
Gurgiolo, C., M. L. Goldstein, A. F. Viñas, and A. N. Fazakerley (2012), Direct observations of the formation of the solar wind halo from the strahl, *Ann. Geophys.*, *30*, 163–175, doi:10.5194/angeo-30-163-2012.
Hollweg, J. V., and H. J. Völk (1970), New plasma instabilities in the solar wind, *J. Geophys. Res.*, *75*(28), 5297–5309, doi:10.1029/JA075i028p05297.
Kennel, C. F., and H. E. Petscheck (1966), Limit on stably trapped particle fluxes, *J. Geophys. Res.*, *71*(1), 1–28, doi:10.1029/JZ071i001p00001.
Lazar, M., and S. Poedts (2009), Firehose instability in space plasmas with bi-Kappa distributions, *A&A*, *494*, 311–315, doi:10.1051/0004-6361:200811109.
Lazar, M., S. Poedts, and R. Schlickeiser (2011), Instability of the parallel electromagnetic modes in Kappa distributed plasmas I. Electron whistler-cyclotron modes, *Mon. Not. R. Astron. Soc.*, *410*, 663–670, doi:10.1111/j.1365-2966.2010.17472.x.
Lazar, M., S. Poedts, and M. J. Michno (2013), Electromagnetic electron whistler-cyclotron instability in bi-Kappa distributed plasmas, *A&A*, *554*, A64, doi:10.1051/0004-6361/201220550.
Lazar, M., S. Poedts, and R. Schlickeiser (2014), The interplay of Kappa and core populations in the solar wind: Electromagnetic electron cyclotron instability, *J. Geophys. Res. Space Physics*, *119*, 9395–9406, doi:10.1002/2014JA020668.
Lazar, M., S. Poedts, R. Schlickeiser, and C. Dumitrache (2015), Towards realistic parametrization of the kinetic anisotropy and the resulting instabilities in space plasmas. Electromagnetic electron-cyclotron instability in the solar wind, *Mon. Not. R. Astron. Soc.*, *446*, 3022–3033, doi:10.1093/mnras/stu2312.
Lazar, M., S. M. Shaaban, S. Poedts, and Š. Štverák (2016), Firehose constraints of the bi-Kappa distributed electrons: A zero-order approach for the suprathermal electrons in the solar wind, *Mon. Not. R. Astron. Soc.*, doi:10.1093/mnras/stw2336, Advance Access on September 15, 2016.
Li, X., and S. R. Habbal (2000), Electron kinetic firehose instability, *J. Geophys. Res.*, *105*, 27,377–27,385, doi:10.1029/2000JA000063.
Maksimovic, M., et al. (2005), Radial evolution of the electron distribution functions in the fast solar wind between 0.3 and 1.5 AU, *J. Geophys. Res.*, *110*, A09104, doi:10.1029/2005JA011119.
Marsch, E. (2006), Kinetic physics of the solar corona and solar wind, *Living Rev. Sol. Phys.*, *3*, 1, doi:10.12942/lrsp-2006-1.
Montgomery, M. D., S. J. Bame, and A. J. Hundhausen (1968), Solar wind electrons: Vela 4 measurements, *J. Geophys. Res.*, *73*, 4999–5003, doi:10.1029/JA073i015p04999.
Moya, P. S, V. Muñoz, J. Rogan, and J. A. Valdivia (2011), Study of the cascading effect during the acceleration and heating of ions in the solar wind, *J. Atmos. Sol. Terr. Phys.*, *73*, 1390–1397, doi:10.1016/j.jastp.2011.01.009.
Moya, P. S., R. Navarro, A. F. Viñas, V. Muñoz, and J. A. Valdivia (2014), Weak Turbulence cascading effects in the acceleration and heating of ions in the solar wind, *Astrophys. J.*, *781*(76), 8, doi:10.1088/0004-637X/781/2/76.
Paesold, G., and A. O. Benz (1999), Electron firehose instability and acceleration of electrons in solar flares, *A&A*, *351*, 741–746.
Pilipp, W. G., H. Miggenrieder, M. D. Montgomery, K.-H. Mühlhäuser, H. Rosenbauer, and R. Schwenn (1987), Unusual electron distribution functions in the solar wind derived from the Helios plasma experiment: Double-strahl distributions and distributions with an extremely anisotropic core, *J. Geophys. Res.*, *92*, 1093–1101, doi:10.1029/JA092iA02p01093.
Samsonov, A. A., O. Alexandrova, C. Lacombe, M. Maksimovic, and S. P. Gary (2007), Proton temperature anisotropy in the magnetosheath: Comparison of 3-D MHD modeling with Cluster data, *Ann. Geophys.*, *25*, 1157–1173.
Schlickeiser, R., M. Lazar, and T. Skoda (2011), Spontaneously growing, weakly propagating, transverse fluctuations in anisotropic magnetized thermal plasmas, *Phys. Plasmas*, *18*(1), 012103, doi:10.1063/1.3532787.
Seough, J. J., and P. H. Yoon (2012), Quasilinear theory of anisotropy-beta relations for proton cyclotron and parallel firehose instabilities, *J. Geophys. Res.*, *117*, A08101, doi:10.1029/2012JA017645.
Seough, J. J., P. H. Yoon, K.-H. Kim, and D. H. Lee (2013), Solar-wind proton anisotropy versus beta relation, *Phys. Rev. Lett.*, *110*(7), 071103, doi:10.1103/PhyRevLett.110.071103.
Seough, J. J., P. H. Yoon, and J. Hwang (2014), Quasilinear theory and particle-in-cell simulation of proton cyclotron instability, *Phys. Plasmas*, *21*, 062118, doi:10.1063/1.4885359.
Seough, J. J., P. H. Yoon, and J. Hwang (2015), Simulation and quasilinear theory of proton firehose instability, *Phys. Plasmas*, *22*, 012303, doi:10.1063/1.4905230.
Shaaban, S. M., M. Lazar, S. Poedts, and A. Elhanbaly (2016), The interplay of the solar wind proton core and halo populations: EMIC instability, *J. Geophys. Res. Space Physics*, *121*, 6031–6047, doi:10.1002/2016JA022587.
Štverák, Š, P. Trávníček, M. Maksimovic, E. Marsch, A. N. Fazakerley, and E. E. Scime (2008), Electron temperature anisotropy constraints in the solar wind, *J. Geophys. Res.*, *113*, A03103, doi:10.1029/2007JA012733.
Štverák, S., M. Maksimovic, P. M. Trávníček, E. Marsch, A. N. Fazakerley, and E. E. Scime (2009), Radial evolution of nonthermal electron populations in the low-latitude solar wind: Helios, Cluster, and Ulysses Observations, *J. Geophys. Res.*, *114*, A05104, doi:10.1029/2008JA013883.
Viñas, A. F., P. S. Moya, R. Navarro, and J. A. Araneda (2014), The role of higher-order modes on the electromagnetic whistler-cyclotron wave fluctuations of thermal and non-thermal plasmas, *Phys. Plasmas*, *21*, 012902, doi:10.1063/1.4861865.
Viñas, A. F., P. S. Moya, R. E. Navarro, J. A. Valdivia, J. A. Araneda, and V. Muñoz (2015), Electromagnetic fluctuations of the whistler-cyclotron and firehose instabilities in a Maxwellian and Tsallis-Kappa-like plasma, *J. Geophys. Res. Space Physics*, *120*, 3307–3317, doi:10.1002/2014JA020554.
Wu, C. S., P. H. Yoon, and H. P. Freund (1989), A theory of electron cyclotron waves generated along auroral field lines observed by ground facilities, *Geophys. Res. Lett.*, *16*, 1461–1464, doi:10.1029/GL016i012p01461.
Xiao, F., Q. Zhou, H. Zheng, and S. Wang (2006), Whistler instability threshold condition of energetic electrons by Kappa distribution in space plasmas, *J. Geophys. Res.*, *111*, A08208, doi:10.1029/2006JA011612.
Yoon, P. H., and J. J. Seough (2012), Quasilinear theory of anisotropy-beta relation for combined mirror and proton cyclotron instabilities, *J. Geophys. Res.*, *117*, A08102, doi:10.1029/2012JA017697.
Yoon, P. H., and J. J. Seough (2014), Proton-cyclotron and firehose instabilities in inhomogeneous plasmas, *J. Geophys. Res. Space Physics*, *119*, 7108–7119, doi:10.1029/2014JA020261.
Yoon, P. H., J. J. Seough, K. H. Kim, and D. H. Lee (2012), Empirical versus exact numerical quasilinear analysis of electromagnetic instabilities driven by temperature anisotropy, *J. Plasma Phys.*, *78*, 47–54, doi:10.1017/S0022377811000407.
Zimbardo, G., A. Greco, L. Sorriso-Vlavo, S. Perri, Z. Vörös, G. Aburjania, K. Chargazia, and O. Alexandrova (2010), Magnetic turbulence in the geospace environment, *Space Sci. Rev.*, *156*, 89–134, doi:10.1007/s11214-010-9692-5.